www.ietdl.org

Published in IET Radar, Sonar and Navigation
Received on 4th June 2013
Revised on 27th September 2013
Accepted on 24th November 2013
doi: 10.1049/iet-rsn.2013.0182

Special Issue: Bistatic and MIMO radars and their applications in surveillance and remote sensing

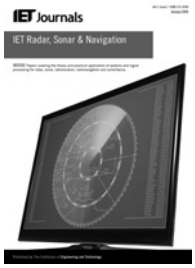

ISSN 1751-8784

Wideband antenna array for Digital Video Broadcast Terrestrial-based passive bistatic radar applications

Daniel W. O'Hagan[1], Martin Schröder[1], Vedaprabhu Basavarajappa[1], Peter Knott[1], Heiner Kuschel[1], Massimilano Simeoni[2]

[1]PSK, Fraunhofer Institute for High Frequency Physics and Radar Techniques FHR, Fraunhoferstrasse 20, 53343 Wachtberg, Germany
[2]European Space Agency (ESA-ESTEC), European Space Research and Technology Centre, Keplerlaan 1, 2200 AG Noordwijk, The Netherlands
E-mail: danieloha@gmail.com

Abstract: A Digital Video Broadcast Terrestrial (DVB-T)-based passive radar requires the development of a dedicated antenna array that performs satisfactorily over the entire DVB-T band. The array should require no mechanical adjustments to the inter-element spacing to correspond to the DVB-T carrier frequency used for any particular measurement. This study describes the challenges involved in designing an ultra high frequency (UHF) antenna array with a bandwidth of 450 MHz. The design procedure is discussed and a number of simulated array configurations are demonstrated. The final configuration of the array will be shown along with the simulations of the expected performance over the desired frequency span. Finally, the actual array is characterised to evaluate its performance based on data from anechoic chamber measurements.

1 Introduction

The subject of passive bistatic radar (PBR) has been comprehensively covered in numerous books and journals, for example, [1, 2]. This paper is concerned with a wideband antenna solution for a Digital Video Broadcast Terrestrial (DVB-T)-based PBR.

The DVB-T frequency band occupies the 470–862 MHz portion of the UHF spectrum. However, to allow for possible variation to the DVB-T broadcast spectrum, the PBR receiver antenna is required to operate between 450 and 900 MHz (i.e. a span of 450 MHz, resulting in a fractional bandwidth of 67%). The actual elements to be used in the PBR antenna array have already been designed and built at Fraunhofer-FHR. They are broad-band discones, cut and tuned to the DVB-T band specifications. A discone antenna is a biconical antenna where one of the cones is replaced by a disc ground plane. The disc is mounted on top of the cone. A full description of the physical and the electrical properties (simulated and measured) of the discone can be found in [3].

The remaining challenge is to appropriately configure the individual discone elements in an array so that the resultant directional antenna can be used to receive all the DVB-T channels between 450 and 900 MHz. The final configuration should be such that no manual adjustments are required for setting the inter-element spacing to correspond to any particular carrier frequency. The design dichotomy, therefore, is to arrange the elements in such a configuration that, on the one hand, the inter-element spacing is not too great to result in grating lobes at the higher frequencies and, on the other hand, not too small to result in strong mutual coupling effects at the lower frequencies.

The bandwidth of a DVB-T channel (in 8 k mode) is 7.61 MHz. It is also important, therefore, to ensure that the phase response of each individual element is closely matched over this bandwidth.

2 Design procedure

Subsequent to the initial investigation of circular arrays, several other array configurations have been explored. This paper shows some of the more realistic configurations. The design procedure has been based on intuition, however, none of these, often more complicated, configurations have performed significantly better than a circular array. It has not been possible because of the project time constraints to pursue an exhaustive array optimisation procedure. However, the authors acknowledge the merit of such a procedure and further work should consider this aspect. Nevertheless, the approach adopted here is grounded on principles known to work. The principles rely on basic array geometries and attempt to make the array perform satisfactorily over the 450–900 MHz span.

As a starting point for the array project, the discone elements have been arranged in an open circular array configuration. Circular arrays are, in general, well suited to passive radar applications. They permit the forming of multiple surveillance beams providing close to a 360° azimuth coverage. Furthermore, one beam can be

designated as a reference and steered directly towards the illuminator of opportunity.

3 Circular array theory

The theory of circular array antennas has been comprehensively covered in textbooks such as [4, 5]. A brief analysis relevant to this work follows.

A circular array far-field radiation pattern can be computed by using the maximum gain weights to create an amplitude taper. The computation assumes that each array element is omnidirectional. The discone elements used in this paper can reasonably be approximated as omnidirectional as they are effectively broadband monopoles with a ground plane. The plots in Fig. 1 show the azimuth radiation patterns for an arbitrary 8-element array of wire dipoles for 450, 675 and 900 MHz, respectively. The inter-element spacing, s, has been taken as 0.4λ (an inter-element spacing less than 0.5λ is sufficient to avoid the grating lobes) at 675 MHz (the centre-band frequency). The array radius is given as

$$r = \frac{Ns}{\lambda k} = \frac{Ns}{2\pi} \tag{1}$$

where N is the number of the array elements and k is the free-space wave-number ($k = 2\pi/\lambda$).

The array radius corresponding to a 0.4λ inter-element spacing at 675 MHz is approximately 0.3 m. It can be seen in Fig. 1 that for the maximum gain weights, the radiation pattern at 450 MHz exhibits one prominent side/backlobe at a level of −8 dB below the peak. This pattern may appear acceptable; however, it is important to note that the effects of mutual coupling have not been included. The mutual coupling is expected to significantly distort the pattern characteristics because of the close inter-element spacing. The plot for 675 MHz represents the case where the inter-element spacing is 0.4λ.

This analysis of circular arrays forms the basis for a more elaborate study of extending the operational bandwidth of circular arrays. Fig. 1 represents the normalised electric field strength against the observation angle and is useful for illustrating the challenge of broadband circular array design.

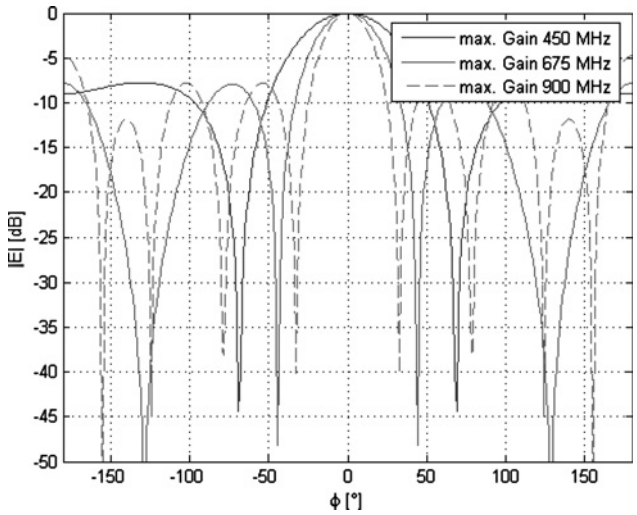

Fig. 1 *Normalised radiation patterns for an arbitrary 8-element array of wire dipoles for 450, 675 and 900 MHz, respectively*
The inter-element spacing, s, is 0.4λ at 675 MHz

4 Broadband array study

Section 3 has considered a theoretical 8-element circular array of dipoles.

A rule of thumb to determine the highest order phase mode, M, that can be excited by the array aperture at a reasonable strength is $M \simeq kr$ where r is the array radius [6].

To satisfy the condition that the principal term of the far-field radiation equation is the dominant term, the highest phase mode excited has order M, and therefore requires

$$N > 2M \tag{2}$$

array elements.

Determining the number of elements in this way is useful from an aperture sampling point of view. Equation (1) determines the array radius from the point of view of having a predefined fixed number of array elements and a predefined inter-element spacing whereas, (2) determines the minimum number of elements to satisfy the aperture sampling conditions when given only a fixed radius. Equation (2) is identical to Nyquist's sampling as M defines the maximum spatial frequency. Therefore to avoid pattern degradation similar to the formation of grating lobes in planar arrays requires adherence to the following condition

$$M \leq 2kr \leq N \tag{3}$$

Fig. 2*a* shows an example computation of the normalised electric field strength of a uniformly distributed 13-element circular array. The radius is 0.45 m and the mainlobe is arbitrarily set at 180°. The array radiation pattern has been computed between 450 and 900 MHz, respectively. It can be seen that as the frequency increases, the sidelobe response begins to deteriorate. However, as expected, no grating lobes are present in the plot as condition (3) has been met.

Fig. 2*b* shows a similar simulation for a 17-element circular array. In this case, the array radius is 0.6 m and the mainlobe has again been set at 180°. The radiation pattern performance for this 17-element array is only slightly better than the 13-element array considered in Fig. 2*a* in terms of exhibiting a lower sidelobe level throughout the entire 450 MHz operational bandwidth.

It is important to note that the effects of mutual coupling have not been considered for either array in Figs. 2*a* and *b*. These examples of the 13-element and the 17-element arrays stem from the aforementioned study of the possible array configurations.

Multiple array configurations have been experimented with. However, as has been noted previously, none have performed substantially better than the uniformly distributed circular arrays previously described. As a result, and subsequent to the hardware and the system constraints, the decision has been taken to focus on an 11-element uniform circular array.

5 Eleven-element uniform circular array

A circular array of 11 broadband discone elements has been chosen for the reasons stated. The inter-element spacing has

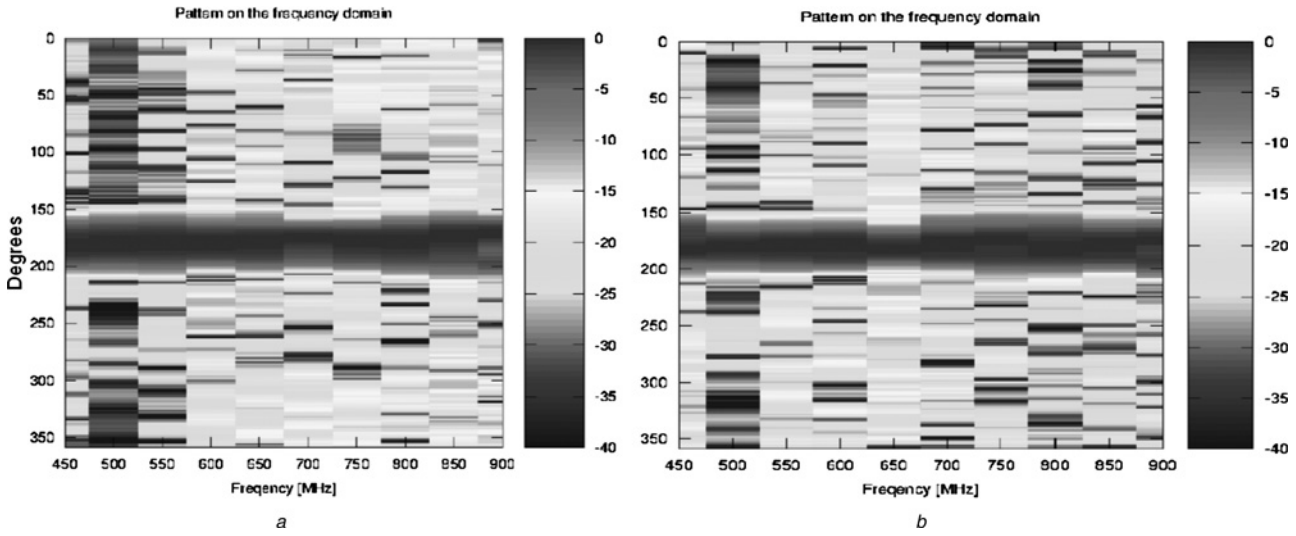

Fig. 2 *Example computation of the normalised electric field strength*

a Normalised radiation pattern simulation from 450 to 900 MHz for a 13-element uniform circular array of dipoles
b Normalised radiation pattern simulation from 450 to 900 MHz for a 17-element uniform circular array of dipoles

been set at 22 cm, measured between the respective geometrical-centres of the consecutive elements. This value of the inter-element spacing has been chosen to satisfy two conditions: to reduce the mutual coupling and to avoid grating lobes. As the discone antenna has a wide 'skirt' angle [3], the actual distance between the edges of the consecutive discones is only 2 cm. The configuration is shown in Fig. 3.

The antenna has been simulated with the electromagnetic solver computer simulation technology (CST) Microwave Studio [7]. The array has a diameter of 77 cm. One of the discone elements has been excited by using a waveguide port whereas the remaining elements have been terminated in matched loads. As the number of mesh cells obtained for the entire 11-element array has approached 90 million cells, a symmetry plane had to be defined to ease the computational burden.

The array arrangement shown in Fig. 3 allows for beamforming and null steering in the 450–900 MHz range. The sidelobe level can be controlled at any desired level in this frequency range.

An LMS (least mean squares) algorithm has been applied iteratively in a sidelobe suppression procedure proposed by Bucci *et al.* [8]. This beamforming method is a constrained

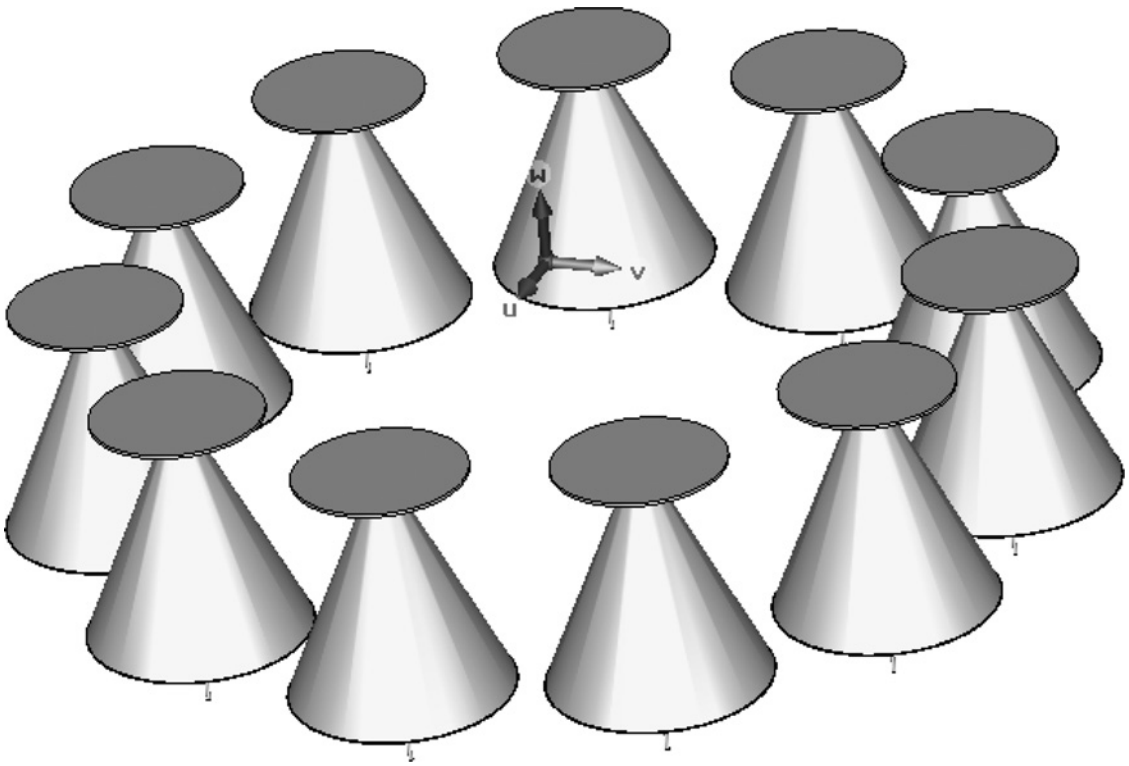

Fig. 3 *Configuration of the 11-element uniform circular array of discone elements*

doi: 10.1049/iet-rsn.2013.0182

iterative LMS optimisation method where the excitation coefficients are determined to 'squeeze' the array radiation pattern (i.e. sidelobe levels) in between two masks representing an upper and a lower limit. If the method does not provide the desired result this can be for different reasons: (a) the number of iterations were too small and the 'optimum' case has not yet been found, or (b) there are some physical limitations owing to the array architecture which make it impossible to achieve the desired goal. Fig. 4 shows an example of the masks defining a desired radiation pattern at 675 MHz.

It is also desirable in passive radar to introduce nulls in the direction of the transmitter to suppress direct signal interference. These nulls should also be steerable in any direction. For illustration purposes, Fig. 5 shows a null introduced in the radiation pattern at 50°. The half-power null-width in this case is approximately 20°.

The null forming method used also utilises the Bucci mask procedure to create a null within the predefined masks at a specified angular direction.

The Bucci method of beamforming to control the sidelobe level and to steer the mainlobe has been computed from 450 to 900 MHz, respectively, in 25 MHz steps. That is, the array coefficients have been calculated for every 25 MHz step

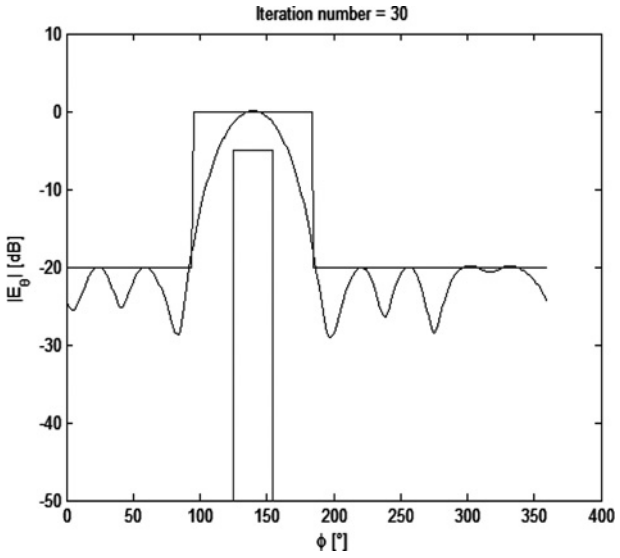

Fig. 4 *Beam steering and sidelobe level control at 675 MHz*

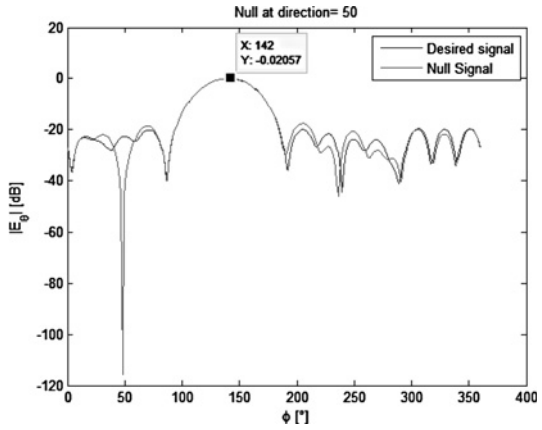

Fig. 5 *Null introduced at 50° while the main beam is directed towards 142°*

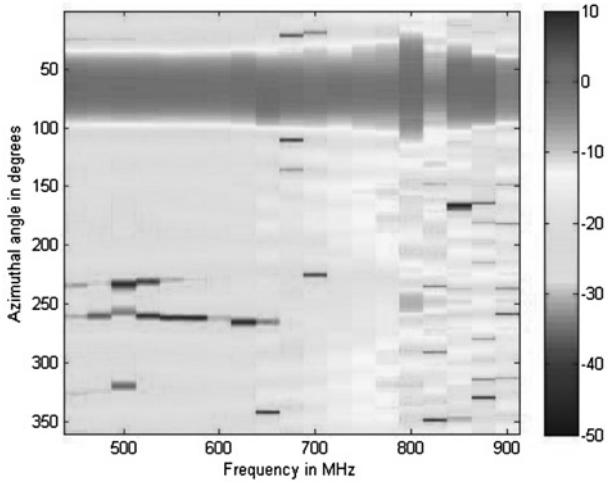

Fig. 6 *Radiation pattern with sidelobe level control and the mainlobe positioning between 450 and 900 MHz, respectively*

between 450 and 900 MHz. Fig. 6 shows the resultant (simulated) array radiation pattern. This simulation has compensated for the effects of mutual coupling, as the coupling coefficients have been obtained from the CST electromagnetic solver. In this case, the mainlobe has been set to 70°.

The beamforming approach described here calculates the array coefficients iteratively before converging to a particular direction. As can be seen from Fig. 6, the choice of $N = 11$ and the adoption of Bucci beamforming has enabled the design of a broadband circular array antenna for DVB-T-based passive radar applications. It can also be seen in Fig. 6 that there are no grating lobes visible over the frequency range of interest.

6 Polarisation considerations

In Germany, DVB-T signals are mostly vertically polarised. It is important for the subsequent array processing, such as beamforming, that the cross-polarised signals are received at a very low level. Fig. 7 shows the results of a simulation using the same excitation coefficients as in Fig. 6 to generate both the co-polarisation and the cross-polarisation patterns.

7 Application to measured data

Based on the results of the tests and the simulations discussed in Sections 4–6, an array of 11 discone elements has been constructed at Fraunhofer-FHR.

Subsequent to the construction, the array underwent comprehensive testing in the anechoic chamber. The array was mounted in a fixed position in the chamber and a log-periodic was used as a probe antenna. A turntable mechanism in the anechoic chamber could rotate the array about the 360° azimuth angular extent. Furthermore, an additional mechanism could rotate the log-periodic probe from 0° to 120° in the elevation angular extent. The resolution of the measurements is as follows:

- 41 elevation angles (from 0° to 120°),
- 120 azimuth angles (from 0° to 360°),
- 801 frequency points (from 450 to 900 MHz),
- Vertical and horizontal polarisations have been measured.

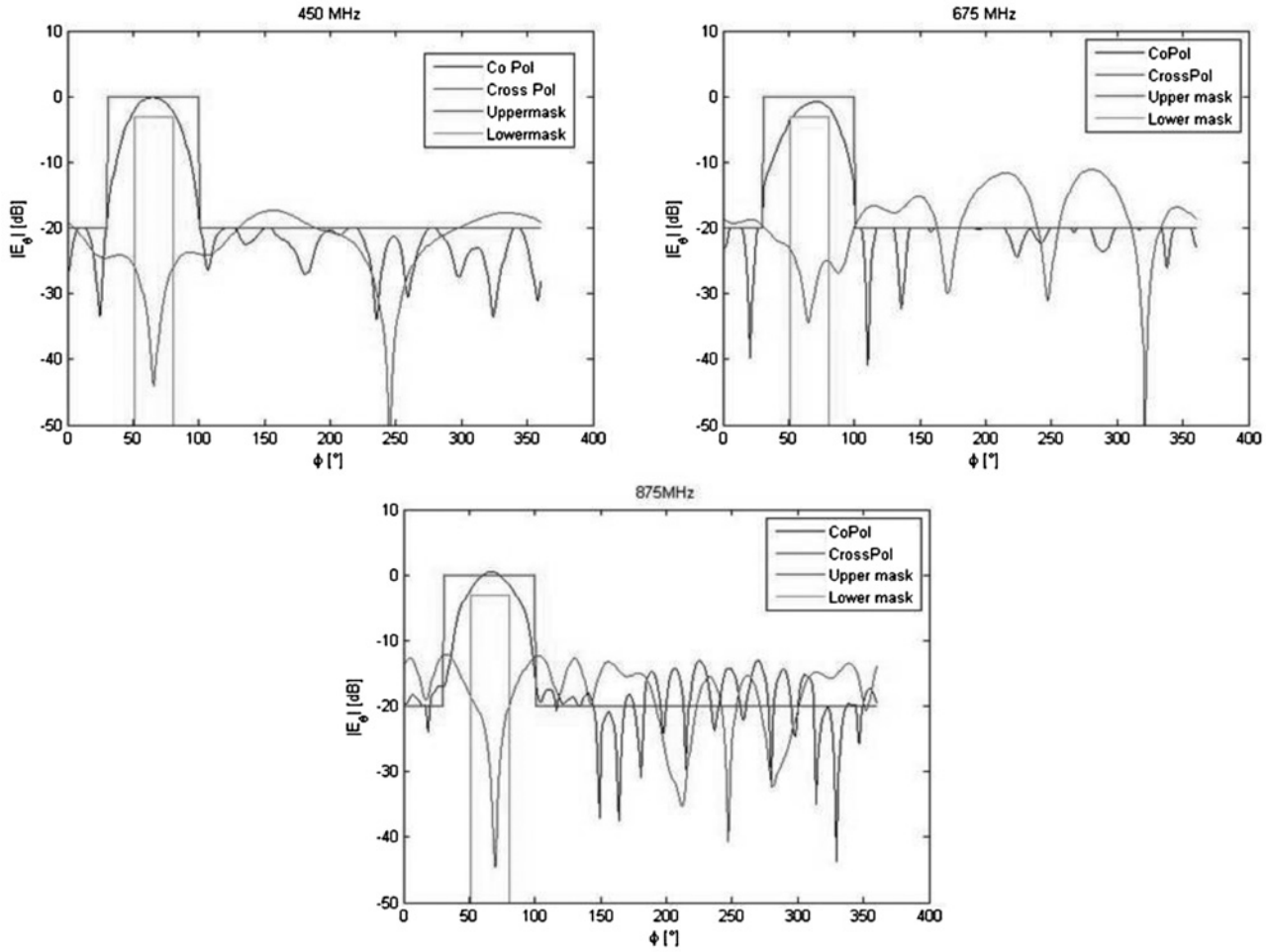

Fig. 7 *Beamforming with the same array excitation coefficients for co-polarisation and cross-polarisation at 450, 675 and 875 MHz, respectively*

The measurement resolutions are the maximum permissible by this particular Orbit anechoic chamber measurement system and are sufficient for observing the array frequency response, the azimuth and the elevation behaviour. The measurement setup is shown in Fig. 8.

The Bucci method of beamforming described in Section 5 has been applied to the measurement data. As a test, the beamforming has been attempted at particular spot-frequencies corresponding to the DVB-T channel carriers. For every carrier frequency, a unique set of beamforming coefficients ensures that the array pattern converges to within the preset mask requirements. Fig. 9 shows an example of the beamforming applied at 578 MHz

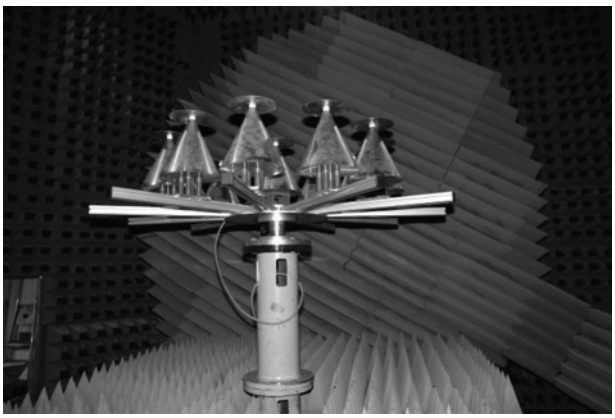

Fig. 8 *Eleven-element circular array mounted in an anechoic chamber*

The array has been rotated 360° in the azimuth and the excitation probe has been moved in the elevation extent from 0° to 120°

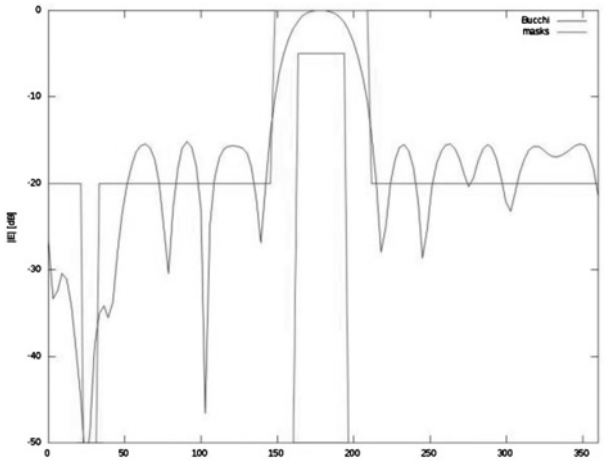

Fig. 9 *Beamforming applied to the measurement data at 675 MHz with the mainlobe in this case steered to 180° and a null introduced at 30°*

doi: 10.1049/iet-rsn.2013.0182

with the mainlobe in this case steered to 180°; furthermore, a null has been introduced at 30° for the suppression of the direct signal interference (DSI).

As the bandwidth of a single DVB-T channel is 7.61 MHz (approximated to 8 MHz for convenience), it is inadequate just to compute the beamforming coefficients for the carrier frequency as the beam pattern will be severely distorted over the width of the DVB-T channel. The Bucci beamforming method applied here has frequency stability over a span of less than 2 MHz. Therefore, intra-channel beamforming coefficients have to be computed to ensure that a pattern distortion does not occur over the 8 MHz channel bandwidth. This important aspect of broadband performance has been compensated for in the array described here. The procedure is best illustrated on a thorough observation of the beamforming applied to the measured data as shown in Figs. 10 and 11.

Fig. 10 shows nine antenna pattern plots. The plot on the top-left corresponds approximately to 4 MHz below the DVB-T carrier frequency under test. The middle pattern in the second row corresponds to the exact carrier frequency under test. The plot on the bottom-right corresponds to approximately 4 MHz above the carrier frequency under test. In this demonstration, the carrier frequency is 578.25 MHz, so the frequency spanned by the nine plots, from the top-left to the bottom-right, is approximately 8 MHz (i.e. $f_c \pm 4$ MHz). In this case, the beamforming coefficients have been calculated for the carrier frequency only and the figure clearly shows how the beamforming performance has deteriorated a few megahertz on either side of the carrier.

Clearly, the pattern response of the array is not acceptable over a channel bandwidth of about 8 MHz, as shown in Fig. 10. The authors have compensated for the distortion so that the array performs to the specified criteria over the channel bandwidth. Rather than simply calculate the beamforming coefficients for the carrier frequency only, a matrix of the coefficients has been calculated for 4 MHz on either side of the carrier in steps of 1 MHz. The intra-channel compensation produces a frequency-stable pattern performance, which is essential in practical application. The resultant (compensated) patterns are shown in Fig. 11. It can be seen that each of the patterns are almost identical. The carrier frequency under test was again 578.25 MHz, however, it is important to note that the beamforming procedure and the compensation perform similarly well for all the design frequencies from 450 to 900 MHz.

A look-up table of beamforming coefficients has been generated for each of the carrier frequencies which the Fraunhofer-FHR DVB-T-based passive radar must currently

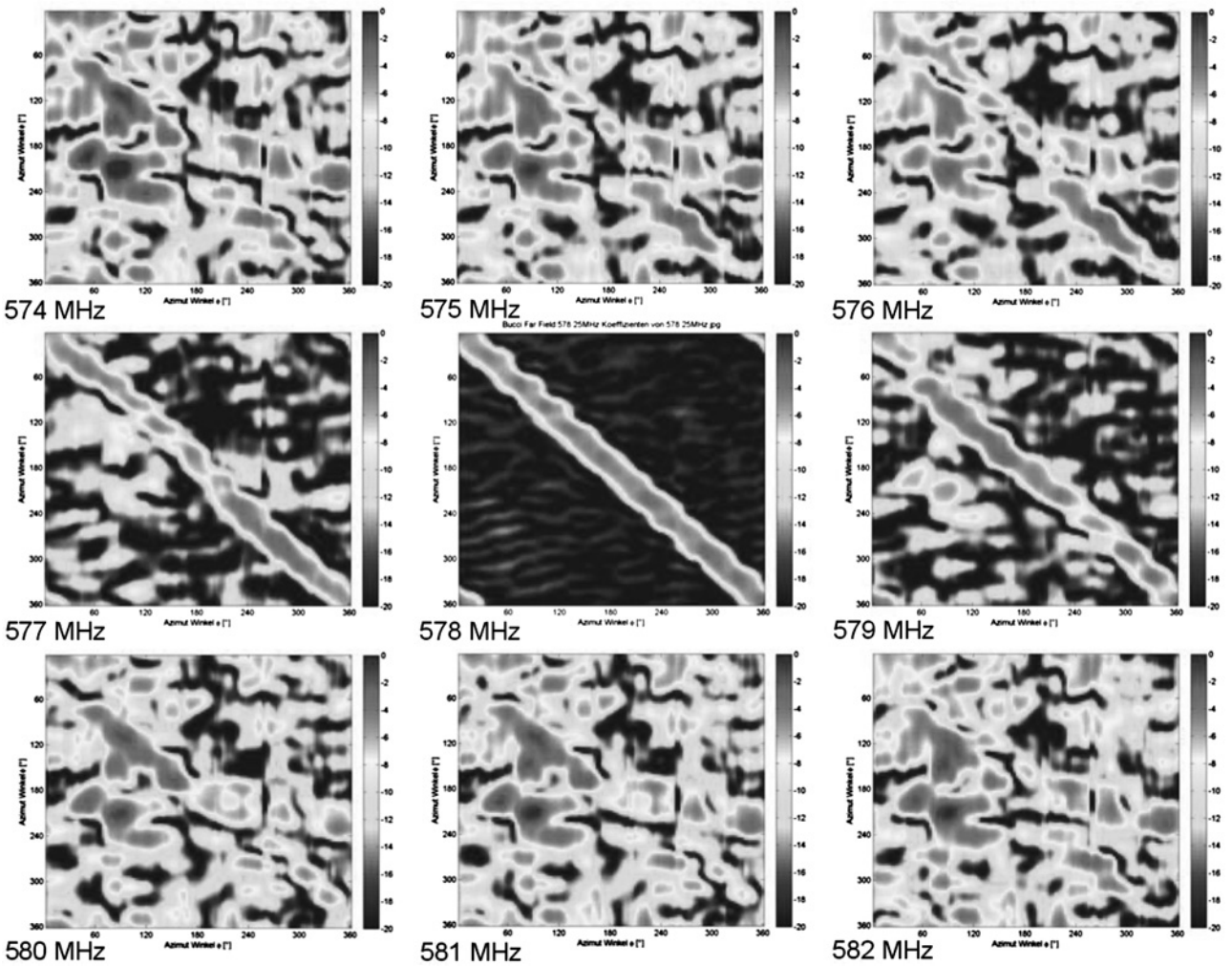

Fig. 10 *In this demonstration, the beamforming coefficients have been calculated for the carrier frequency only (in this example 578.25 MHz)*

The figure clearly shows how the beamforming performance has deteriorated a few megahertz on either side of the carrier
The frequency spanned by the nine plots, from the top-left to the bottom-right, is approximately 8 MHz (i.e. $f_c \pm 4$ MHz)

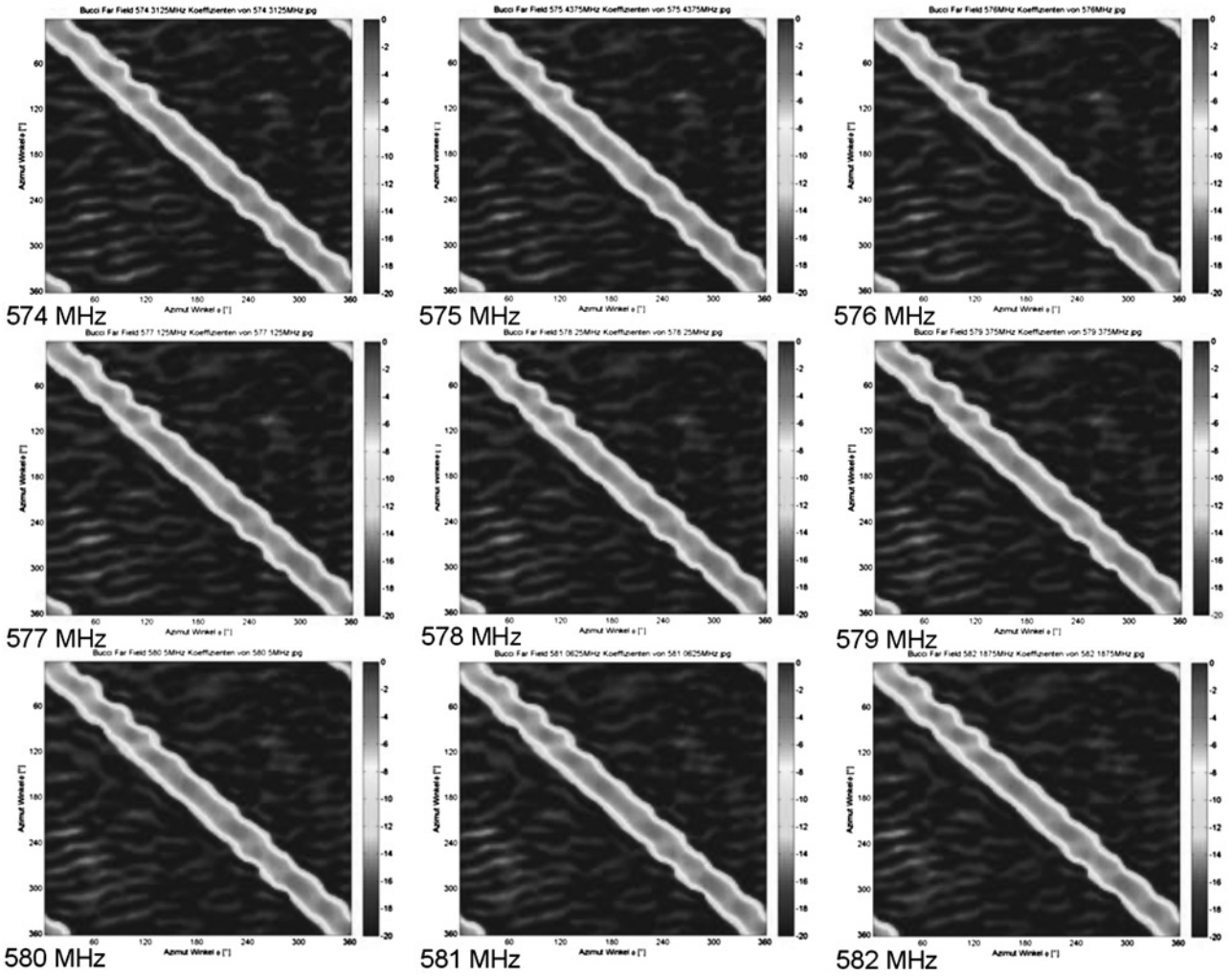

Fig. 11 *The intra-channel compensation produces a frequency-stable pattern performance*

Here, the beamforming coefficients have been calculated for 4 MHz on either side of the carrier in steps of 1 MHz ($f_c = 578.25$ MHz)
It can be seen that each of the patterns are almost identical and the distortion reported in Fig. 10 has been eliminated

utilise. More carriers, indeed every carrier in the DVB-T band, could easily be added to the look-up table as required without additional computational demands on the radar. Furthermore, the intra-channel compensation is inherent to the procedure to ensure frequency stability over the DVB-T channel bandwidths.

8 Conclusions and future work

This paper has characterised a wideband circular antenna array from conception through simulation, construction and test. The discone elements neatly conform to the predefined broadband specifications [3]. The early work has concentrated on the most appropriate arrangement of the elements to achieve a broadband operation over the DVB-T operating band. As has been demonstrated, the 11-element circular array with an inter-element spacing of 22 cm (from the centre of each cone) has yielded satisfactory performance in terms of low sidelobes and no grating lobes over the frequency extent from 450 to 900 MHz. The choice of 11 elements has been governed by hardware limitations. The beamforming and null-steering have been simulated and have also been applied to the measurement data, as demonstrated in Figs. 10 and 11.

The array has been comprehensively measured (shown in Fig. 8) in the anechoic chamber. The results conform to the theoretical expectations. It has been shown that intra-channel compensation has been required to ensure that beamforming remains stable over a span of about 8 MHz (the approximate width of a single DVB-T channel). It is important to note that the intra-channel compensation is not required when using DAB illuminators as their channel bandwidths are 1.5 MHz. A similar array to the one described here is being used in an FHR DAB-based passive radar demonstrator.

Finally, the array here is currently an integral component of the CORA-11 passive radar demonstrator (Fraunhofer-FHR). The array is robust and lends itself well as a platform on which to experiment with novel signal processing approaches. The agility and the performance of the array on a number of field trials will be the subject of a subsequent paper to accompany this.

9 References

1 Willis, N.J., Griffiths, H.D.: 'Advances in bistatic radar' (Scitech Publishing Inc., USA, 2007)
2 Colone, F., O'Hagan, D.W., Lombardo, P., Baker, C.J.: 'A multistage processing algorithm for disturbance removal and target detection in

doi: 10.1049/iet-rsn.2013.0182

passive bistatic radar', *IEEE Trans. Aerosp. Electron. Syst.*, 2009, **45**, (2), pp. 698–722
3 Knott, P., Nowicki, T., Kuschel, H.: 'Design of a disc-cone antenna for passive radar in the DVB-T frequency range'. German Microwave Conf. (GeMiC), Darmstadt, Germany, March 2011
4 Davis, D.E.N.: 'The handbook of antenna design' (Peter Peregrinus Ltd., London), 1983, **2**, (12), pp. 298–327
5 Josefsson, L., Persson, P.: 'Conformal array antenna theory and design' (Wiley-Interscience Publication, 2006)
6 Steyskal, H.: 'Digital beamforming aspects of wideband circular arrays'. IEEE Aerospace Conf., 1–8 March 2008, pp. 1–6
7 http://www.cst.com
8 Bucci, O.M., Mazzarella, G., Pannariello, G.: 'Array synthesis with smooth excitation'. IEEE Antennas & Propagation Society Symp., 7–11 May 1990, pp. 856–859